



# Kinematic and dynamic analysis of an anatomically based knee joint

Kok-Meng Lee\*, Jiajie Guo

The George W. Woodruff School of Mechanical Engineering, Georgia Institute of Technology, Atlanta, GA 30332-0405, USA

## ARTICLE INFO

### Article history:

Accepted 2 February 2010

### Keywords:

Bio joint  
Sliding velocity  
Exoskeleton  
Dynamic model

## ABSTRACT

This paper presents a knee-joint model to provide a better understanding on the interaction between natural joints and artificial mechanisms for design and control of rehabilitation exoskeletons. The anatomically based knee model relaxes several commonly made assumptions that approximate a human knee as engineering pin-joint in exoskeleton design. Based on published MRI data, we formulate the kinematics of a knee-joint and compare three mathematical approximations; one model bases on two sequential circles rolling a flat plane; and the other two are mathematically differentiable ellipses-based models with and without sliding at the contact. The ellipses-based model taking sliding contact into accounts shows that the rolling-sliding ratio of a knee-joint is not a constant but has an average value consistent with published measurements. This knee-joint kinematics leads to a physically more accurate contact-point trajectory than methods based on multiple circles or lines, and provides a basis to derive a knee-joint kinetic model upon which the effects of a planar exoskeleton mechanism on the internal joint forces and torque during flexion can be numerically investigated. Two different knee-joint kinetic models (pin-joint approximation and anatomically based model) are compared against a condition with no exoskeleton. The leg and exoskeleton form a closed kinematic chain that has a significant effect on the joint forces in the knee. Human knee is more tolerant than pin-joint in negotiating around a singularity but its internal forces increase with the exoskeleton mass-to-length ratio. An oversimplifying pin-joint approximation cannot capture the finite change in the knee forces due to the singularity effect.

© 2010 Elsevier Ltd. All rights reserved.

## 1. Introduction

With rapid advances in robotics and mechatronics, exoskeletons have been widely developed to assist in or rehabilitate human body motions; for examples, the commercialized Lokomat (Colombo et al., 2000) for treadmill training, assistant exoskeleton (Kiguchi et al., 2003) for elderly persons, hybrid assistive limb (Kawamoto and Sankai, 2005) to assist in walking and climbing, the ankle-foot orthosis powered by artificial pneumatic muscles (Ferris et al., 2005), and the Berkeley lower extremity exoskeleton (Zoss et al., 2006) to assist in carrying heavy loads over rough terrain. Experiments (Gordon and Ferris, 2007) on a robotic exoskeleton controlled by muscle activity could be useful tools for testing neural mechanism of human locomotor adaptation. While mechanical exoskeletons have the advantages of adding energy to human motions and adjusting motion patterns, it could perturb normal motions and potentially cause pains or even damages to human joints. To minimize negative effects of an artificial exoskeleton on human joints, the design and control of rehabilitation exoskeletons

require a good understanding of the natural bio-joint kinematics and kinetics.

Natural bio-joints (that exoskeletons are designed to rehabilitate) are commonly modeled in kinematics as non-slip revolute joints (such as a pin or ball joint). Unlike an engineering joint which typically has a fixed rotational center, bio-joints often consist of non-uniform shaped contact parts that roll and slide. Human bodies also vary widely in shapes and sizes and change over years; engineering joints are usually not compliant to accommodate these variations. Although exoskeletons help users adapt their motion after repetitive training, there are potentials for damages to bio-joints in long term usage if natural joint variations are not accounted for.

Compliant mechanisms that reduce assembled joints (and thus friction) can be employed in exoskeleton to accommodate (shape, size and motion) variations in human joints. “Soft” pneumatic muscle actuators (pMA) are used as power sources (Tsagarakis and Caldwell, 2003), and flexible cables are used for transmission in LOPES (Veneman et al., 2006). However, most of the works on compliance have been motivated by power efficiency rather than the interaction between a human body and an exoskeleton. Recent works also concern about shock absorption; for example, flexible geared joint and rubber footpad (Low, 2005). Besides gaining energy, an exoskeleton should not interfere negatively

\* Corresponding author. Tel.: +1 404 8947402.

E-mail address: [kokmeng.lee@me.gatech.edu](mailto:kokmeng.lee@me.gatech.edu) (K.-M. Lee).

with normal human-joint motions; otherwise, it could result in discomfort and potential damages. For these reasons, problems on interaction between bio-joints and compliant mechanism are worthy of exploration.

Among challenges in the modeling of human body motion are the characterization of the joint mechanics and musculoskeletal geometry (Pandy, 2001). Different experimental methods have been developed to detect joint structures, and measure the knee joint motions (Bull and Amis, 1998). These include the most commonly used skin-marker systems (Lafortune et al., 1992; Lu and O' Connor, 1999) where soft tissues often make them difficult to apply, and the radiation softographic/fluoroscopic techniques (Peterfy et al., 2003; Li et al., 2008). More recently, the electromagnetic techniques (MRI) (Iwaki et al., 2000) provide a way to shed light on the internal geometries of joints. With geometrical details of a joint available from experiments, kinematic models can be built for analyses. A computer model with surface friction (Sathasivam and Walker, 1997) was suggested showing that the condylar geometries could have important differences in kinematics, function and wear. Accurate solutions of tibiofemoral contact behavior were obtained from a 3D finite-element model (Donahue et al., 2002). Recently, a computational model allowing for anatomical details was built using CAD/CAE methods to predict the lower leg kinematics (Liacouras and Waynel, 2007).

Motivated by the need to provide a good understanding on the interaction between natural joints and artificial mechanisms for design and control of rehabilitation exoskeletons, this paper introduces a mathematical bio-joint model originally proposed (Lee and Guo, 2008) for mechanical deboning of chicken breast meat (Guo and Lee, 2008). The remainder of this paper offers the followings:

- We formulate an anatomically based model for characterizing a human knee joint so that its internal joint forces/torques during flexion can be accurately analyzed. The bio-joint model relaxes several assumptions commonly made on a knee joint in exoskeleton design.
- Two examples are given. The first investigates the effects of different bio-joint geometrical approximations (with/without sliding) on the contact locations. The second numerically investigates the effects of a planar exoskeleton on a human knee joint by comparing two different models for predicting the forces/torque acting on the knee; pin-joint approximation and bio-joint model.

2. Methods

With MRI data, a model can be built to provide a good understanding of the kinematics and kinetics of a bio-joint (consisting of non-uniform shaped contact parts), and estimate its contact locations, rolling/sliding velocities and forces/torques involved.

Fig. 1(a) shows a lateral sagittal MRI of an unloaded cadaver knee (Iwaki et al., 2000), where the two white circles are approximated geometries for the femoral articular surfaces. Data are presented as positions of the extension facet center (EFC) and flexion facet center (FFC) in Fig. 1(a), where the contact is modeled as a point between a circle and a plane. To provide a continuous differentiable function, a more general bio-joint representation based on elliptical geometries is proposed in Fig. 1(b) to characterize the observed data for analyzing the contact kinematics and kinetics, where  $\Omega_A$  and  $\Omega_B$  are two bodies with surfaces  $\Gamma_A$  and  $\Gamma_B$ , respectively; and the angular velocity  $\omega$  describes the motion of  $\Omega_A$  rolling on  $\Omega_B$  at the instantaneous contact point C.

2.1. Knee joint kinematics

Given a contact point on  $\Gamma_A$ , there always exists a tangential plane with a normal vector  $\mathbf{n}$  such that the angular velocity  $\omega$  describes the motion of  $\Omega_A$  at the contact point. An instantaneous osculating plane perpendicular to this tangent

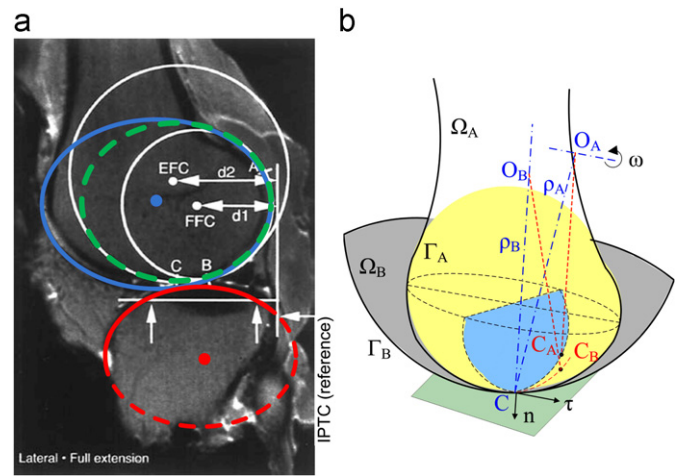


Fig. 1. Bio-joint illustration: (a) MRI of a cadaver knee (Iwaki et al., 2000) where the two ellipses approximate the contact regions of the knee. (b) Bio-joint model (Lee and Guo, 2008) for analyzing the contact kinematics based on elliptical geometries.

plane can then be defined as shown in Fig. 1(b) to characterize the 3D motion of a biological joint, which depends on the location of the contact point (and hence is a function of time). The contact points on  $\Gamma_A$  and  $\Gamma_B$  move incrementally from  $C_A$  and  $C_B$  to C along the respective osculating circles, where  $(O_A, \rho_A)$  and  $(O_B, \rho_B)$  are the centers and radii of the osculating circles intersecting at  $\Gamma_A$  and  $\Gamma_B$ , respectively. The rotation axis changes with the contact point as  $\Omega_A$  rolls and slides on  $\Omega_B$ .

For the knee joint in Fig. 1(a), the normal component (along  $\mathbf{n}$ ) of the angular velocity is generally nonzero but very small as compared to the component on the tangent plane, and thus neglected to simplify the bio-joint kinematic analysis. The 3D kinematics of a biological joint is reduced to finding the contact location in the motion of the osculating circle and the position and orientation of  $\Omega_A$ . The rolling velocity  $v_{roll}$  due to the angular velocity about the rotation center  $O_A$  is defined in Eq. (1) as follows:

$$v_{roll}(\theta) = \omega \rho_A \quad \text{where } \omega = d\theta/dt \tag{1}$$

For a specified ellipse,  $\rho_A$  is a function of the contact position (Lee and Guo, 2008; Davis and Snider, 1987). As observed in published data (Iwaki et al., 2000), the sliding velocity  $v_{slide}$  also depends on the flexion angle  $\theta$  as

$$v_{slide}(\theta) = \frac{ds_{slide}}{dt} = \omega \frac{ds_{slide}}{d\theta} \tag{2}$$

where  $s_{slide}$  is the difference between the rolling displacement  $s_{roll}$  (or integrated  $v_{roll}$  over  $\theta$ ) and the path length of the contact point from the MRI data.

Using a lumped-parameter approach in polar coordinates  $(r, \theta)$  where the reference ( $\theta=0$ ) is along the longitudinal axis of the femur (Fig. 2), the lower limb (leg and foot) is modeled as a mass centered at O. As illustrated in Fig. 2(b) where  $C_i$  is the initial contact point on the femur, the distance  $r_0$  from the center of the lateral tibial condyle to O is a constant; and C is measured from the ipsilateral posterior tibial cortices (IPTC). The bio-joint kinematics can be computed from the following:

$$\dot{r} = \omega \frac{dr}{d\theta}; \quad \text{and } \ddot{r} = \dot{\omega} \frac{dr}{d\theta} + \omega^2 \frac{d^2r}{d\theta^2} \tag{3a, b}$$

where  $r$  provides a means to account for the change in the rotational center. Engineering ball joints are special cases where both spherical surfaces are concentric and hence,  $\dot{r} = \ddot{r} = 0$ . The (mass center O) trajectory can be computed in terms of  $\theta$  from the following:

$$\mathbf{r} = r \mathbf{e}_r; \quad \mathbf{v} = \dot{r} \mathbf{e}_r + r \dot{\theta} \mathbf{e}_\theta \tag{4a, b}$$

$$\mathbf{a} = (\ddot{r} - r \dot{\theta}^2) \mathbf{e}_r + (2\dot{r} \dot{\theta} + r \ddot{\theta}) \mathbf{e}_\theta \tag{4c}$$

2.2. Knee joint dynamics

The calf dynamics (relative to the upper leg) are given by

$$m \mathbf{a} = \mathbf{f}_g + \mathbf{f}_\theta + \mathbf{f}_r + \mathbf{f}_e \tag{5a}$$

$$(\dot{J} \ddot{\theta} + 2m r \dot{\theta} \dot{\theta}) \mathbf{k} = \boldsymbol{\tau}_g + \boldsymbol{\tau}_\theta + \boldsymbol{\tau}_e \quad \text{where } \mathbf{k} = \mathbf{e}_r \times \mathbf{e}_\theta \tag{5b}$$

where  $m$  is the calf mass;  $\mathbf{f}_g$  is the gravity force; and  $\mathbf{f}_r$  and  $\mathbf{f}_\theta$  are the resultant forces exerted by the surrounding bones and tissues (muscle and ligament) in  $\mathbf{e}_r$

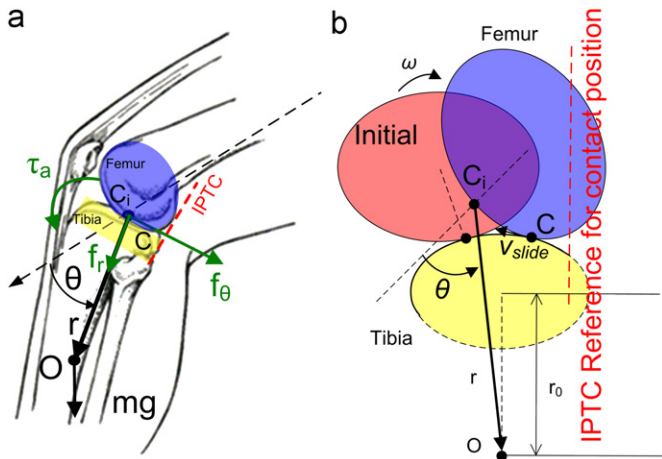


**Fig. 2.** Coordinates illustrating the knee joint rotation: (a) the tibia rotation in polar coordinates centered at the initial contact point  $C_i$ . (b) Schematics illustrating the relationship between the distance  $r$  and flexion angle  $\theta$ .

and  $e_\theta$  directions, respectively. Within a bio-joint, bones primarily support compressive forces; and soft tissues can only exert tensile forces. For example,  $f_r$  represents the force from the tissues if tensile force dominates, or otherwise from the bones. With rehabilitation applications in mind, we include  $f_e$  to account for the force exerted by an external device (such as an exoskeleton) and reaction from the ground. On the left hand side of Eq. (5b), the 1st term accounts for the moment-of-inertia  $J$  (about  $C_i$ ) due to the leg rotation while the 2nd term describes the interaction between  $\theta$  and  $\dot{r}$  due to the variation in  $r$ . In Eq. (5b), all the torques are computed about  $C_i$ :  $\tau_g$  and  $\tau_e$  denote the torques due to the gravity and external device, respectively; and  $\tau_a$  is a net torque accounting for  $f_r$ ,  $f_\theta$ , and tissue contraction within the knee.

The vector Eqs. (5a, b) can be recast into three scalar equations (6a, b, c) from which  $f_r$ ,  $f_\theta$  and  $\tau_a$  can be solved as

$$m(\ddot{r} - r\dot{\theta}^2) = f_g \sin \theta + f_r + f_{er}(\theta) \tag{6a}$$

$$m(2\dot{r}\dot{\theta} + r\ddot{\theta}) = f_g \cos \theta + f_\theta + f_{e\theta}(\theta) \tag{6b}$$

$$J\ddot{\theta} + 2mr\dot{\theta} = \tau_g + \tau_a + \tau_e(\theta) \tag{6c}$$

### 3. Results and discussion

Two sets of results are presented here. The 1st set investigates the effect of the geometrical approximations on the contact (between the femoral and tibial articular surfaces) with published data (Iwaki et al., 2000) as a basis for comparison. The 2nd set illustrates the effects of an exoskeleton on the human knee joint.

#### 3.1. Effect of bio-joint models on contact point trajectory

In (Iwaki et al., 2000), two circles, each of which rolls on a different flat facet, were used for the sagittal section of the medial tibiofemoral compartment but for the lateral tibiofemoral compartment, two circles roll on the same flat facet. In this paper, the simulations focus on the lateral part as it has a larger displacement than the medial part. The following three models are compared:

Model 1: Two sequential circles roll on a flat plane (Iwaki et al., 2000).

Model 2: One ellipse rolls on a flat plane.

Model 3: One ellipse rolls on another ellipse.

The dimensions of the approximated circles and ellipses (Fig. 1b) are listed in Table 1. With the contact location defined as a horizontal distance of  $C$  measured from the IPTC in Fig. 1(a), results are given as a function of the flexion angle  $\theta$  in Fig. 3 for comparing three models against published data. Fig. 4 simulates

**Table 1**  
Geometry approximation.

Circles (Iwaki et al., 2000)		Ellipse (green dash)	
$r_1=21$ mm	$r_2=32$ mm	$r_{maj}=25.3$ mm	$r_{min}=21.1$ mm
Ellipse (blue)		Ellipse (red)	
$r_{maj}=33.6$ mm	$r_{min}=23$ mm	$r_{maj}=28.8$ mm	$r_{min}=18.8$ mm
Initial contact position=31 mm;			
Angular velocity $\omega=1.57$ rad/s			

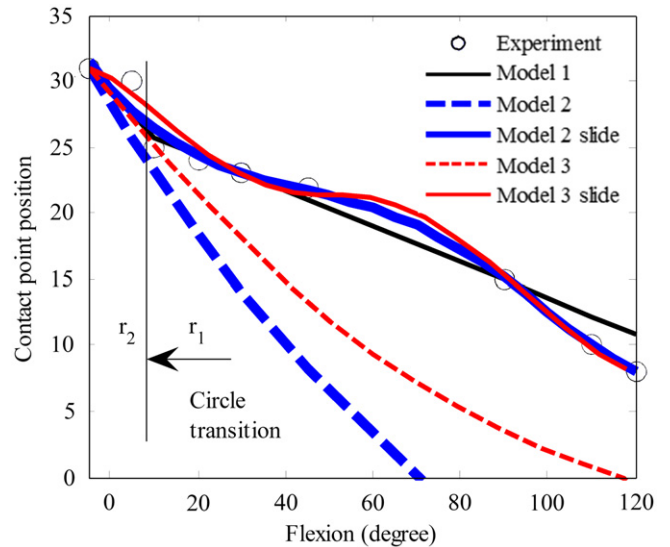


**Fig. 3.** Comparison of current contact point  $C$  positions between different models showing the sliding effect in the knee rotation.

(on the basis of Model 3) the snap-shot trajectory of the lower leg as it rotates from its initially full extension, and its corresponding (rolling/sliding) displacements, velocities as well as the  $s_{roll}/s_{slide}$  ratio. Observations in Figs. 3 and 4 are discussed as follows:

- For Model 1, the  $s_{roll}/s_{slide}$  ratio is given as 1.7. As the sliding velocity of each rolling circle is assumed constant, the contact point is a linear function of  $\theta$ . The overall result, however, is not a smooth curve (Fig. 3) due to the transition from circles  $r_2$  to  $r_1$ . The difference between the 2-circle model and experimental results can be observed when  $\theta > 90^\circ$ . This is because the rotational axis of the circle is tilted by a small angle; when projected on the camera plane, the tilted circle is essentially as an ellipse.
- Based on the above observation, we model bio-joints using elliptical surfaces as they offer a more realistic characterization than a multi-circle model, and are mathematically differentiable. Fig. 3 compares Models 2 and 3 against published data. With only rolling, Model 2 (that simplifies the tibial condyle as a planar surface) results in some negative contact positions; this is intuitively incorrect as the knee joint does not lose contact. Given the close match between Model 3 (when considering both sliding and rolling in the joint kinematics) and the experimental data, Model 3 with sliding is used for the subsequent analysis.
- The displacements,  $s_{roll}(\theta)$  and  $s_{slide}(\theta)$ , normalized to the major radius of the femoral condyle, are given by Eqs. (7a) and (b), respectively, and their ratio is plotted in Fig. 4(b):

$$s_{roll}(\theta)/r_{maj} = 0.093\theta^5 - 0.409\theta^4 + 0.57\theta^3 - 0.448\theta^2 - 0.926\theta \tag{7a}$$

$$s_{slide}(\theta)/r_{maj} = 0.334\theta^5 - 1.518\theta^4 + 2.12\theta^3 - 0.996\theta^2 + 0.513\theta \tag{7b}$$

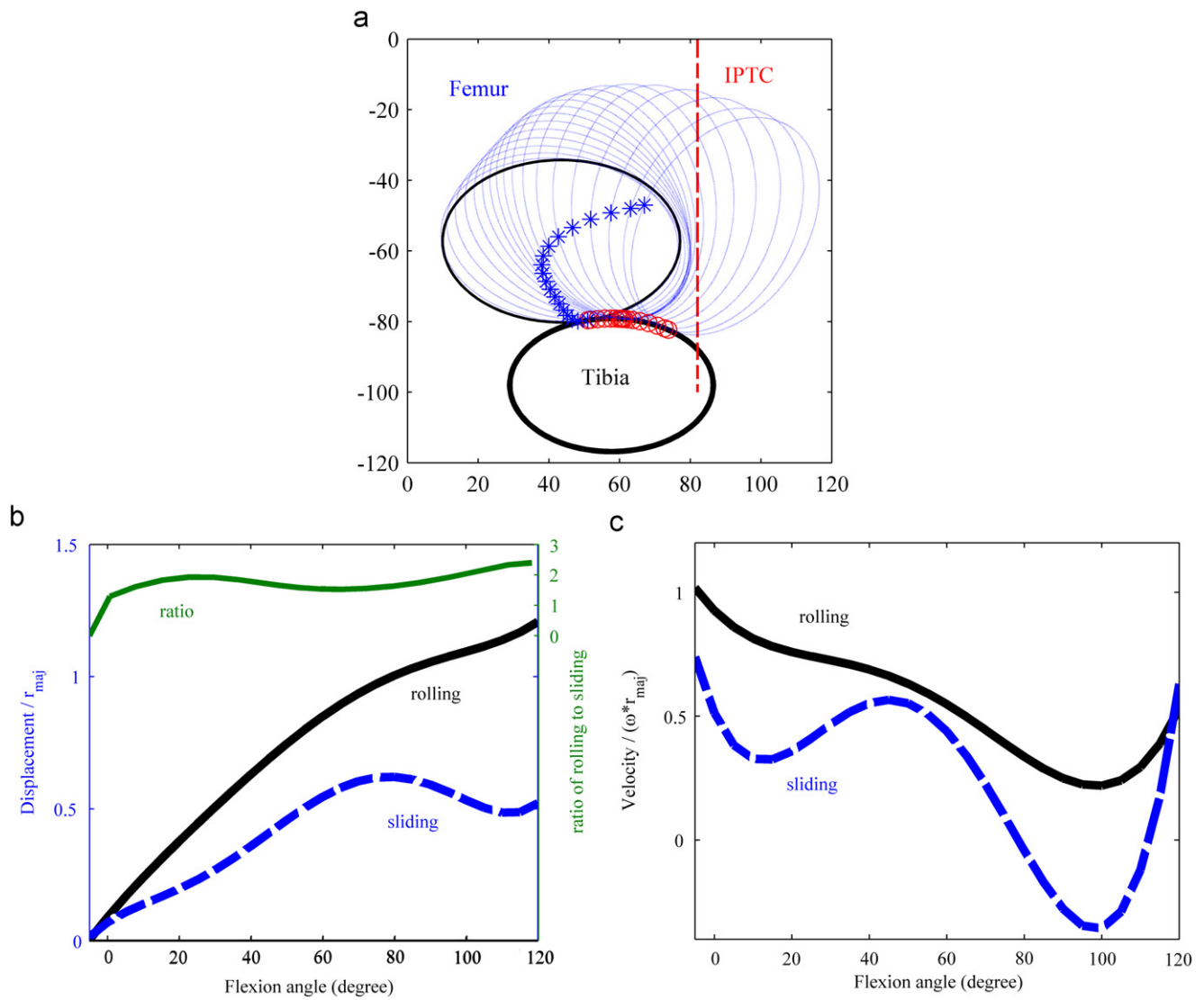


**Fig. 4.** Rolling and sliding velocities of the current contact point (Model 3): (a) snapshots of the femoral condyle and position changes of initial/current contact points. (b) Plots of normalized rolling and sliding displacements showing their ratio is not a constant. (c) Plots of normalized rolling and sliding velocities as the knee rotates at a constant speed (90°/s).

**Table 2**  
Physical parameters of human's lower leg.

	Human		Exoskeleton length (m)
	Length (m)	Mass (kg)	
Upper leg	0.40	7.02	0.40
Lower leg/foot	0.37/0.27	2.44/1.18	0.37
r <sub>0</sub> (m)	0.2453		

The  $v_{roll}/v_{slide}$  ratio is not a constant, but its average value of 1.69 closely agrees with the experimental observation (Iwaki et al., 2000) of 1.7. Fig. 4(c) graphs  $v_{slide}$  calculated from Eq. (2); negative  $v_{slide}$  means sliding forward instead of backward.

**3.2. Effect of exoskeleton design on joint forces/torque**

Due to the kinematic constraint imposed by the contact, the human knee joint embodies two degrees of freedom (DOF), rotation and translation for its planar motion. To investigate the

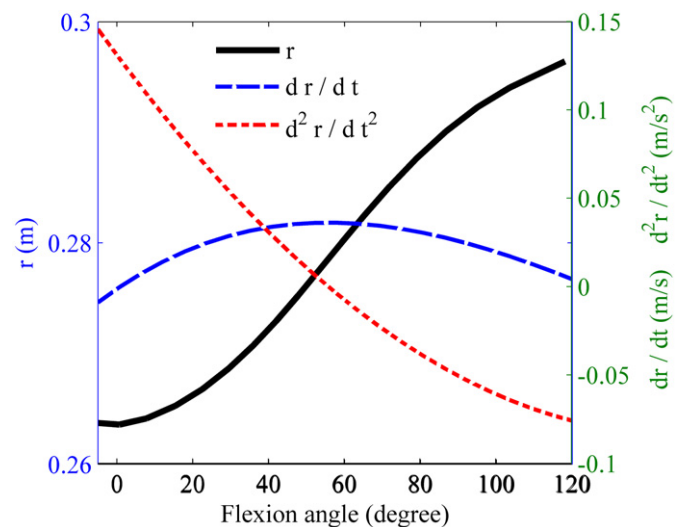


**Fig. 5.** Distance, velocity and acceleration of the tibia mass-center during knee rotation.

effects of a planar exoskeleton on human knee joints, we compare two different models in predicting the forces and moments acting on the knee; namely,

- Pin-joint (PJ) engineering approximation and
- Bio-joint knee (BJK) Model 3.

The exoskeleton consists of a revolute (pin) joint between two rigid links attached to the lower and upper legs with pin joints. This design has three-DOF from its three pin-joints and thus has one redundancy. For a nonzero flexion angle, there are two possible solutions. However, only one solution is physically feasible.

For clarity and ease of illustration, the following assumptions are made: (1) the human subject sits with the upper leg held static and horizontal and the lower link rotates with the tibia from its initial state (full extension); and (2) the lower link is attached at  $O$  with the revolute joint centered at the initial contact point  $C_i$

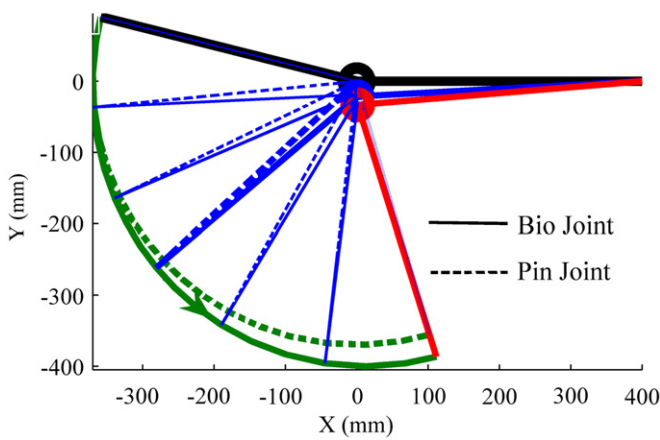


Fig. 6. Comparing snapshots of an exoskeleton between two different knee joint models.

(Fig. 2). Numerical values used in this study are given in Table 2 (Nomiya et al., 2007) and from Figs. 2(b) and 4(a),

$$r(\theta) = 1.078\theta^4 - 11.184\theta^3 + 26.542\theta^2 - 0.825\theta + 263.59 \quad (8)$$

Eq. (8) and its derivatives are graphed in Fig. 5. Fig. 6 shows the link kinematics (solid lines) as the tibia rotates, where dash lines simulate the knee as a pin joint (commonly assumed in exoskeleton designs) for comparison.

To account for the exoskeleton mass in the kinetic study, the two links are assumed to have the same mass-to-length ratio  $\eta$  of 0.5 kg/m. Unlike the condition with no exoskeleton where the human leg is an open-chain mechanism, the leg and exoskeleton form a closed kinematic chain that has a significant effect on the internal joint forces and torque of the knee. Fig. 7(a–c) are calculated results from Eq. (6) showing the internal forces and torque in the knee as the tibia accelerates from the initial static state ( $\theta = -5^\circ$ ) to  $\theta = 20^\circ$  for 0.5 s, then maintains at an angular velocity for 1 s to  $\theta = 95^\circ$ , and finally decelerates to the final static state  $\theta = 115^\circ$  in another 0.5 s. Throughout the trajectory, the foot is off the ground and thus, there is no ground reaction. In Fig. 7 where the solid and dashed lines are results of the BJK and PJ models, respectively, the internal forces and torque for a condition with no exoskeleton are plotted as a basis for comparison.

Several observations can be made from Figs. 5–7:

1. The sign of the force  $f_r$  in Fig. 7(a) can be explained as follows. During the initial flexion ( $\theta < 0$ ),  $f_r$  is positive since the force is primarily supported by the femur, but becomes negative as the retraction force from the soft tissues gradually plays a more dominant role as the knee rotates downward.
2. The distance  $r$  increases as much as 30 mm (Fig. 5). For the same work done, this increase in  $r$  tends to reduce  $f_r$  in the knee. As the PJ approximation assumes a constant  $r$  and neglects the joint geometry, the effect of the  $r(\theta)$  variation on the attaching point (Fig. 6) and on the forces/torque (Fig. 7) cannot be accounted for. As compared to the BJK model in Fig. 7(a), the PJ approximation overestimates  $|f_r|$  in the range ( $0^\circ < \theta < 90^\circ$ ) and underestimates as  $\theta$  approaches its rotation limit.

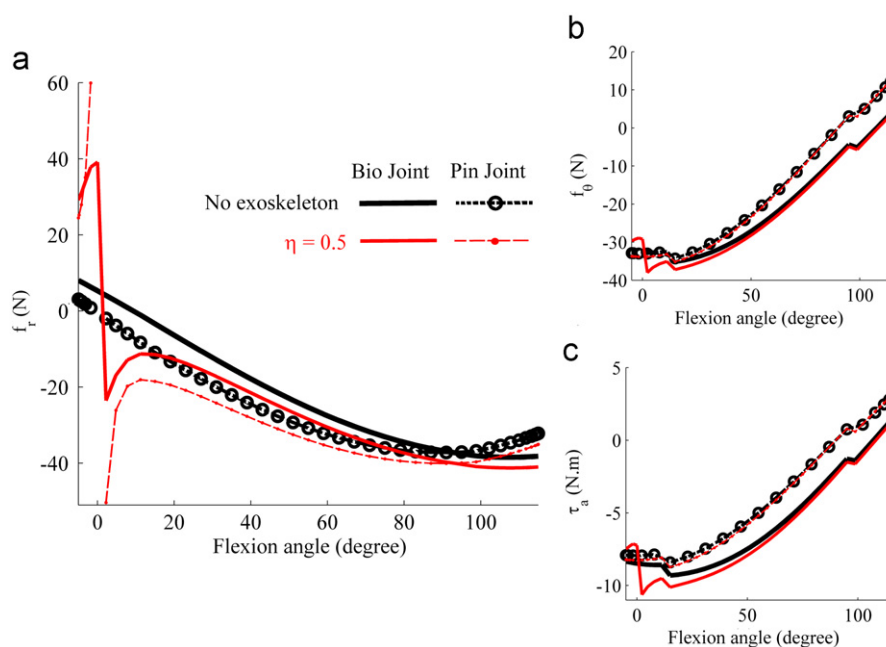


Fig. 7. Force and torque comparison between two different knee joint models with/without exoskeleton: (a) pin-joint knee approximation overestimates  $f_r$  in the range  $-5^\circ < \theta < 90^\circ$  and underestimated in  $\theta > 90^\circ$  as compared to the bio-joint knee model. (b) Tangential force  $f_\theta$ . (c) Moment  $\tau_a$ .

3. Near  $\theta=0^\circ$ , the exoskeleton loses one DOF along the  $\mathbf{e}_r$  direction causing a finite change in  $f_r$  as well as  $f_\theta$  and  $\tau_a$  as shown in Fig. 7. Human knee (that can roll and slide) is more tolerant than a pin-joint to a singularity along  $\mathbf{e}_r$  as illustrated in Fig. 7(a). However, these internal forces and torque increase with the mass-to-length ratio  $\eta$  of the exoskeleton. An increase in  $\eta$  from 0.5 to 1 kg/m implies that  $f_r$  (at  $\theta=0^-$ ,  $\theta=0^+$ ) would increase from (39N, -24N) to (73N, -51N). The PJ approximation, which neglects the  $r(\theta)$  variation, cannot capture the finite change in  $f_r$  and also grossly underestimates the singularity effect on  $f_\theta$  and  $\tau_a$ .
4. The trapezoidal-velocity  $\theta$  trajectory (commonly used in robotics) has an effect on the tangential force  $f_\theta$  and moment  $\tau_a$ . As seen in Fig. 7(b) and (c), the two sudden changes at  $\theta=20^\circ$  and  $\theta=95^\circ$  (on the simulated  $f_\theta$  and  $\tau_a$ ) are reactions from the soft tissues in order to meet the acceleration changes specified in the  $\theta$  trajectory.

#### 4. Conclusions

A general method for mathematical modeling a bio-joint has been introduced, which provides a better understanding on the interaction between natural joints and artificial mechanisms for design and control of rehabilitation exoskeletons. With the aid of MRI data (Iwaki et al., 2000), the ellipsoid-based bio-joint model has been shown to offer a physically more accurate account of both rolling and sliding motion within bio-joint than a geometrically simple pin-joint approximation or methods based on multiple circles and lines. The bio-joint model shows that the sliding-rolling displacement ratio is not a constant but has an average value consistent with published measurements and its mathematically differentiable property facilitates the analysis of rolling/sliding velocity. Finally, the effects of a planar exoskeleton on a human knee joint have been numerically illustrated by comparing results of two different knee models (pin-joint approximation and bio-joint model derived from published MRI data). A single-DOF pin-joint approximation (that oversimplifies the knee joint geometry) cannot account for the effect of the translational variation on the attaching point of the exoskeleton, and on the internal forces and torque in the knee. While a detailed exoskeleton design to accommodate joint flexibility of a knee is beyond the scope of this paper, some intuitive insights presented here are potentially useful considerations for future design of rehabilitation exoskeletons.

#### Conflict of interest statement

The authors declare that they have no conflict of interest.

#### Acknowledgment

The project is partially funded by the Georgia Agricultural Technology Research Program.

#### References

- Bull, A.M.J., Amis, A.A., 1998. Knee joint motion: description and measurement. In: Proceedings of the Institution of Mechanical Engineers, Part H, Journal of Engineering in Medicine 212(5), 357–372.
- Colombo, G., Joerg, M., Schreier, R., Dietz, V., 2000. Treadmill training of paraplegic patients using a robotic orthosis. Journal of Rehabilitation Research and Development 37 (6), 693–700.
- Davis, H., Snider, A.D., 1987. Introduction to Vector Analysis 5th ed. Wm.C., Brown, Dubuque, IA.
- Donahue, T.L.H., Hull, M.L., Rashid, M.M., 2002. A finite element model of the human knee joint for the study of tibio-femoral contact. ASME Journal of Biomechanical Engineering 124 (3), 273–280.
- Ferris, D.P., Czerniecki, J.M., Hannaford, B., 2005. An ankle-foot orthosis powered by artificial pneumatic muscles. Journal of Applied Biomechanics 21 (2), 189–197.
- Gordon, K.E., Ferris, D.P., 2007. Learning to walk with a robotic ankle exoskeleton. Journal of Biomechanics 40 (12), 2636–2644.
- Guo, J., Lee, K.-M., 2008. Effects of musculoskeleton model on flexible deboning automation. In: International Symposium on Flexible Automation, 23–26 June 2008, Atlanta GA, USA.
- Iwaki, H., Pinskerova, V., Freeman, M.A.R., 2000. Tibiofemoral movement 1: the shapes and relative movements of the femur and tibia in the unloaded cadaver knee. Journal of Bone and Joint Surgery 82-B, 1189–1195.
- Kawamoto, H., Sankai, Y., 2005. Power assist method based on phase sequence and muscle force condition for HAL. Advanced Robotics 19 (7), 717–734.
- Kiguchi, K., Iwami, K., Yasuda, M., Watanabe, K., Fukuda, T., 2003. An exoskeletal robot for human shoulder joint motion assist. IEEE/ASME Transactions on Mechatronics 8 (1), 125–135.
- Lafortune, M.A., Lambert, C.E., Lake, M.J., 1992. Skin marker displacement at the knee joint. In: Proceedings of the 2nd North American Congress on Biomechanics, Chicago, IL, August 24–28.
- Lee, K.-M., Guo, J., 2008. Biological joint kinematic model for flexible deboning automation. In: International Symposium on Flexible Automation, 23–26 June 2008, Atlanta GA, USA.
- Li, G.A., de Velde, S.K.V., Bingham, J.T., 2008. Validation of a non-invasive fluoroscopic imaging technique for the measurement of dynamic knee joint motion. Journal of Biomechanics 41 (7), 1616–1622.
- Liaccouras, P.C., Waynel, J.S., 2007. Computational modeling to predict mechanical function of joints: application to the lower leg with simulation of two cadaver studies. ASME Journal of Biomechanical Engineering 129 (6), 811–817.
- Low, K.H., 2005. Initial experiments on a leg mechanism with a flexible geared joint and footpad. Advanced Robotics 19 (4), 373–399.
- Lu, T.W., O' Connor, J.J., 1999. Bone position estimation from skin marker coordinates using global optimisation with joint constraints. Journal of Biomechanics 32 (2), 129–134.
- Nomiyama, T., Lawi, A., Katsuhara, T., Hirokawa, S., 2007. Model Analysis of Lower Limb at Deep Knee Flexion. In: Proceedings of the International Conference on Electrical Engineering and Informatics, 17–19 June 2007, Institut Teknologi Bandung, Indonesia.
- Pandy, M.G., 2001. Computer modeling and simulation of human movement. Annual Review of Biomedical Engineering 3, 245–273.
- Peterfy, C., Li, J., Zaim, S., Duryea, J., Lynch, J., Miaux, Y., Yu, W., Genant, H.K., 2003. Comparison of fixed-flexion positioning with fluoroscopic semi-flexed positioning for quantifying radiographic joint-space width in the knee: test-retest reproducibility. Skeletal Radiology 32 (3), 128–132.
- Sathasivam, S., Walker, P.S., 1997. A computer model with surface friction for the prediction of total knee kinematics. Journal of Biomechanics 30 (2), 177–184.
- Tsagarakis, N.G., Caldwell, D.G., 2003. Development and control of a “soft-actuated” exoskeleton for use in physiotherapy and training. Autonomous Robots 15 (1), 21–33.
- Veneman, J.F., Ekkelenkamp, R., Kruidhof, R., van der Helm, F.C.T., 2006. A series elastic- and Bowden-cable-based actuation system for use as torque actuator in exoskeleton-type robots. International Journal of Robotics Research 25 (3), 261–281.
- Zoss, A.B., Kazerooni, H., Chu, A., 2006. Biomechanical design of the Berkeley lower extremity exoskeleton (BLEEX). IEEE/ASME Transactions on Mechatronics 11 (2), 128–138.